PROGRESS
IN COLOR, COLORANTS AND COATINGS

available online @ www.pccc.icrc.ac.ir

Progress in Color Colorants Coating 18 (2025), 397-408

Ministry of Science, Research and Technology
Institute for Color Science & Technology

Corrosion Behavior and Characteristics of HA+CSZ Nano Bio Composite Coating Prepared by EPD

M. H. Abdulkareem, A. Dhahir Subhi, A. M. Mustafa*, H. Ali Hussein, I. Adnan Annon, A. Thamer Mohammed
Production Engineering & Metallurgy Department, University of Technology, P.O. Box: 35010, Baghdad, Iraq.

ARTICLE INFO

Article history:
Received: 04 Feb 2025
Final Revised: 17 Apr 2025
Accepted: 26 Apr 2025
Available online: 21 July 2025

Keywords:
Biomedical applications
Hydroxyapatite
Nanocomposites
CSZ
Corrosion resistance

ABSTRACT

This study successfully demonstrated the electrophoretic deposition (EPD) of a biocomposite coating comprised of hydroxylapatite (HA) and calcia stabilized zirconia (CSZ) onto 316L stainless steel substrates. The research investigated the influence of varying CSZ concentrations (1-3 %) while maintaining a constant HA concentration of 3 g/L in the EPD solution, focusing on how these variations affected the coating's overall characteristics. A combination of analytical techniques-including adhesion strength testing, cyclic polarization, X-ray diffraction (XRD), and scanning electron microscopy (SEM)-was employed to thoroughly characterize the as-deposited coatings. The results revealed that the inclusion of CSZ significantly improved the coating's properties. Coatings exhibited low porosity and high crystallinity, which contributed to enhanced electrochemical performance and robust adhesion to the substrate. Measured coating thicknesses increased from 9.26 μm at 1 % CSZ to 11.11 μm at 2 % CSZ, and further to 14.34 μm at 3 % CSZ. Additionally, the corrosion resistance of the coated samples was markedly improved with the incorporation of CSZ, accompanied by a decrease in the wettability angle and an increase in adhesion strength as the CSZ concentration was raised. These findings suggest that optimizing CSZ content in HA-based biocomposite coatings could be a promising strategy for enhancing the durability and performance of stainless steel implants. Prog. Color Colorants Coat. 18 (2025), 397-408© Institute for Color Science and Technology.

1. Introduction

Corrosion is a critical factor affecting the longevity and performance of metallic implants in biomedical applications [1]. The interaction between the implant material and the physiological environment often leads to the degradation of the material, compromising its structural integrity and potentially leading to implant failure [2, 3]. To address these challenges, surface modification techniques have been employed to enhance the corrosion resistance and biocompatibility of metallic implants [4, 5].

One promising approach is the application of nano biocomposite coatings, which combine the beneficial properties of different materials at the nanoscale [6]. Among these, Hydroxyapatite (HA) is widely recognized for its excellent biocompatibility and osteoconductivity, making it a preferred choice for bone-related applications. However, HA alone may not provide sufficient corrosion protection, particularly in aggressive physiological environments [7-10].

*Corresponding author: * Ali.m.mustafa@uotechnology.edu.iq
https://doi.org/10.30509/pccc.2025.167464.1361

The hydroxyapatite is a major component of calcium orthophosphate family, also known as HA, with chemical formula of $Ca_{10}(PO_4)_6(OH)_2$. It exhibits a number of noteworthy properties such as neutral pH, chemical stability, and osteoconductivity including biocompatibility, and the ability to bind to bones [10-13]. The HA coating on metallic implant surfaces, such stainless steel, Titanium (Ti), and magnesium (Mg) alloys, which, under physiological conditions, can simultaneously boost the bioactivity and corrosion resistance of implants, is significantly required in orthopedic applications [14-16]. Plasma spray, micro-arc oxidation, electrodeposition, sol gel and magnetron sputtering deposition are used as some of HA coating technologies [17]. On the other hand, electrophoretic deposition (EPD) technology is increasingly being used due to its great advantages. These advantages can be represented by being a simple process, operating at moderate temperature, being applicable to complex substrates, and being highly productive [18-20]. Unfortunately, poor adhesion strength is the common shortcoming of EPD [21]. The significant advantages of EPD have attracted researchers to overcome the shortcomings and enhance the characteristics of EPD coatings. Adding oxide particles, such as zirconia (ZrO_2), into the HA coating is an option to overcome the EPD coating challenges [22, 23]. Generally, zirconia has outstanding characteristics such as high mechanical properties, good biocompatibility, strong wear and corrosion resistance. Incorporating zirconia particles into hydroxyapatite (HA) coatings has been shown to enhance mechanical properties, biocompatibility, and corrosion resistance, making it beneficial for biomedical applications through reducing degradation rate and ion release [24-27]. Calcium-stabilized zirconia (CSZ) is an advanced form of zirconia obtained by incorporating calcium oxide (calcia) as a stabilizing agent [28]. It is reported that CSZ contributes to enhance the corrosion resistance of the coating by providing a more stable barrier that protects the underlying substrate from corrosive agents in bodily fluids. Furthermore, CSZ enhances biocompatibility by promoting favorable cellular responses, such as increased cell adhesion and proliferation, which supports better integration with bone tissue [29]. Therefore, CSZ applied through electrophoretic deposition (EPD) can significantly enhance the characteristics of coatings, especially for biomedical applications [30-32]. There is little information known about the effect of CSZ concentration on the corrosion behavior of HA coatings using EPD [33, 34]. Therefore, this work will shed some light on the effect of CSZ concentration associated with constant concentration of HA on the characteristics of EPD coating especially corrosion resistance and bioactivity in vitro. The microstructure, phases and hardness were also investigated in this work.

2. Experimental

2.1. Samples preparation

The chemical composition of 316L stainless steel used as a substrate was illustrated in Table 1. The samples were cut with dimensions 10×20×2 mm. The surface roughness of the substrate was reduced to Ra 2.63 nm using sandblasting with TiO_2 abrasive grit. The samples were cleaned using an ultrasonic processor (Mixsonix Incorporated, New York, USA) for 10 min after washing with ethanol. Before deposition, the substrate was thoroughly washed with distilled water after pickling in 20 % HNO_3 for 10 min to remove oxide layer from the substrate.

2.2. EPD of HA/CSZ coating

Figure 1 shows a flow chart of the EPD suspension formation. This is done by dispersing chitosan used as a binder at a concentration (0.5 g/L) prepared by dissolving 0.05 g of chitosan in 1 % acetic acid. The yield was added to a solution of 94 % ethanol (purity 99.8 %) + 5 % deionized water, then 3 g/L of hydroxyapatite (HA) with different percentages of 50 nm CSZ nanopowder (1, 2 and 3 %) was added.

Table 1: Chemical composition of 316L stainless steel.

Element	C	Si	Mn	P	S	Cr	Mo	Ni	Al	Co	Cu	Nb
Wt. %	0.015	0.578	1.35	0.043	0.008	16.8	1.97	9.35	0.003	0.221	0.244	0.005
Element	Ti	V	W	Ta	N	Sn	Pb	Se	Sb	others	Fe	-
Wt. %	0.011	0.039	0.037	0.01>	0.041	0.011	0.003	0.005	0.003>	0.001>	Remain	-

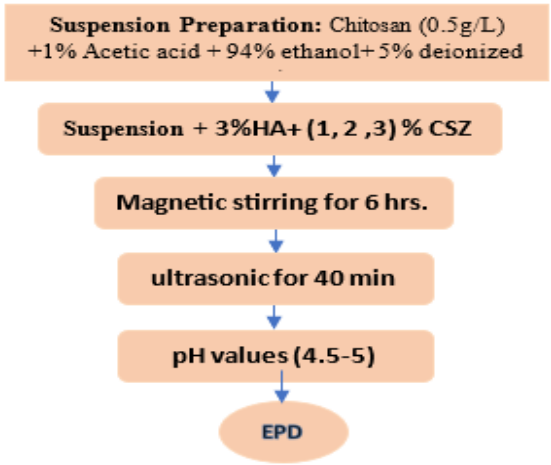

Figure 1: Flowchart of suspension formation for EPD.

The solution was stirred by magnetic stirrer for 6 h and then mixed using ultrasonic for 40 min at room temperature. The pH values of all solutions were fixed between 4.5-5. A 316L stainless steel substrate was used as the cathode and anode electrode. The electrodes were connected to a DC power source and placed parallel to each other within a space of 10 mm. The EPD was performed at 40 V for 5 min at 30 °C. The coatings were then allowed to dry in air for 24 h at room temperature.

2.3. Coating characterization

The microstructural analysis of the EPD coatings was conducted using both optical microscopy (OM) and scanning electron microscopy (SEM, TESCAN-VEGA/USA) to examine cross-sectional morphology. Phase composition was determined via X-ray diffraction (XRD) using a Shimadzu XRD-6000 (Japan) with monochromatic CuKα radiation, scanning at a rate of 0.02°/s over a 2Θ range of 10-90°. The zeta potential of the suspensions was measured using the Brookhaven Nano-Brook Zeta-Plus method, which employs phase analysis light scattering (PALS) to assess particle mobility and electrostatic interactions, providing insight into coating adhesion to the substrate. Additionally, the wettability of the coatings was evaluated by measuring the contact angle of a sessile drop of distilled water on the substrate surface.

2.4. Corrosion study in simulated body fluid (SBF)

The electrochemical measurements of corrosion parameters were made for HA+1 % CSZ, HA+2 % CSZ and HA+3 % CSZ coatings on 316L stainless steel, in a cyclic polarization mode in SBF at room temperature. The SBF was prepared according to ISO 10993.15 by dissolving reagent grade chemicals: $(NH_2)_2CO$ (0.13gL), NaCl (0.7gL), $NaHCO_3$ (1.5gL), Na_2HPO_4 (0.26 gL), K_2HPO_4 (0.2gL), KSCN (0.33gL), and KCl (1.2gL). A three-electrode cell setup was used including a platinum electrode as a counter and Ag/AgCl as a reference electrode. All tests were performed using a potentiostat/ galvanostat (PCI4/750, GAMRY, Inc., Warminster, PA).

The samples were maintained in an open circuit (OCP) for 30 minutes before the experiment. Using a scan range of 700 to 1800 mV and a potential change rate of 2 mV/s, a cyclic polarization test was performed. Using the Tafel extrapolation method, the corrosion potential (E_{corr}) and corrosion current density (i_{corr}) were calculated from the polarization curves.

2.5. Contact angles test

A contact angle goniometer (Creating Nanotechnology Tech., Model: CAM110P, Serial No. 113031201804W) and a CCD camera were used at room temperature to measure the water contact angles for the HA+1 % CSZ, HA+2 % CSZ, and HA+3 % CSZ coatings. All measurements were repeated twice.

2.6. Bonding strength test

The resistance of a coating to detachment from the substrate and its adhesion properties can be analyzed using three methods: the pull test, the cross-hatch test, and the scrape adhesion test. In the cross-hatch test, a specialized tape is firmly placed over the cross-hatch pattern and then quickly removed by pulling it back. This procedure reveals the amount of coating lifted by the tape. The detachment area is then determined using ImageJ v.154k software.

3. Results and Discussion

3.1. Solution stability (zeta potential)

Table 2 illustrates the zeta potential and mobility of the solutions used to create the coatings for HA/CSZ layers. Controlling the deposition of coatings requires an understanding of electrophoretic mobility values. The interaction between ceramic and polymer particles during deposition is essential for controlling the EPD process of organic-inorganic composite coatings that are particularly pertinent for biomedical applications. The fact that there are substantial absolute values of zeta potential, which denote excellent stability, the

presence of a well-dispersed suspension, and also foreshadow a cathodic deposition, suggests that all suspensions are suitable for EPD. Additionally, the mobility increases with the increase of the absolute value of zeta potential. Because the adsorption of chitosan might result in a larger charge and higher zeta-potential, the increased concentration of CSZ nano-particles leads to better electrophoretic mobility.

3.2. Structure and morphology of coatings

The topographic microstructure of the HA+1%CSZ coatings is depicted in Figure 2a and 3a obtained by OM and SEM, respectively. Both types of coatings show signs of cracking. Larger cracks are evident in HA+2 % CSZ as in Figure 2 b and 3 b. These cracks could develop as a result of wetness evaporation, the growth from amorphous to the crystalline phase, and the shrinking of coating and Grain agglomerates separated by a lot of pores make up HA+ 3 % CSZ coatings. At relatively low electrochemical potentials during EPD, solution particles cannot adequately migrate or form a homogeneous coating. The extra time and movement required to locate and occupy the ideal location to produce a uniform coating explains the greater number of agglomerates shown in HA+3 % CSZ Figures 2c and 3c.

Figure 4 shows the X-ray diffraction (XRD) patterns of the HA-CSZ coatings. The XRD patterns show HA and CSZ peaks for all coatings. The γ-Fe appears in all XRD patterns of the coatings due to the thin coating that allows easy penetration of X-ray into the surface of 316L stainless steel. It is reported that HA enhances the bioactivity of the implant material [35]. It is clear that the main peak of γ-Fe is observed at diffraction plane of (111) that corresponding to diffraction angle (2θ) of 43.76°. On the other hand, a family of HA planes such as (211), (300), (222), (200) and (213) produce diffraction peaks at diffraction angles (2θ).

Table 2: Zeta potential values for different solutions.

Solution	Zeta potential (mV)	Mobility $m^2/(V \cdot s)$
Chitosan	30.78	0.61
1 g/L CSZ+3 g/L HA+0.5 g/L chitosan	5.28	0.1
2 g/L CSZ+3 g/L HA+0.5 g/L chitosan	35	0.7
3 g/L CSZ+3 g/L HA+0.5 g/L chitosan	62	1.24

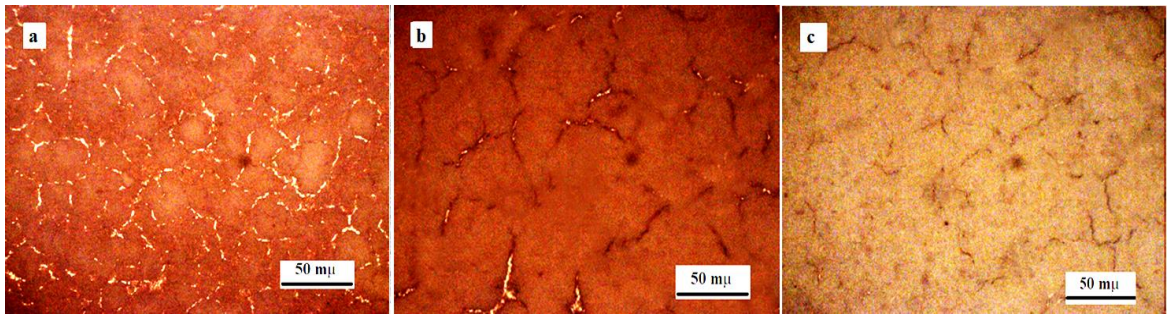

Figure 2: OM images of (a) HA+1 % CSZ (b) HA+2 % CSZ) and (c) HA+3 % CSZ coatings.

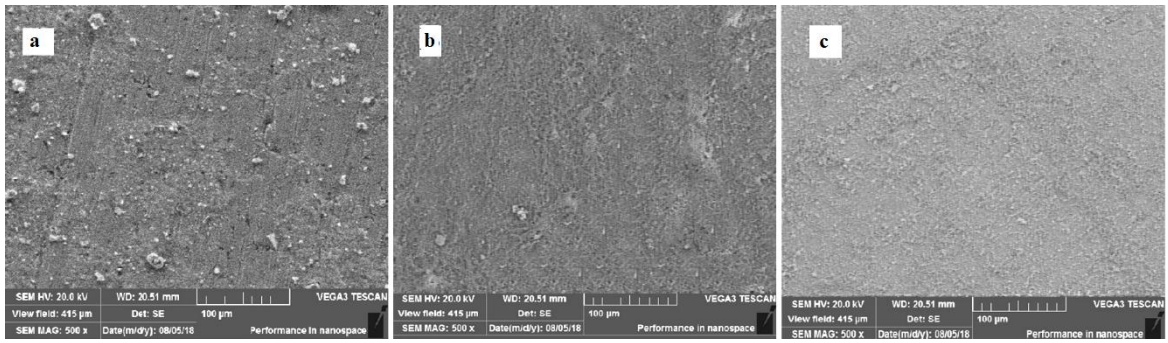

Figure 3: SEM images of (a) HA+1 % CSZ (b) HA+2 % CSZ) and (c) HA+3 % CSZ coatings.

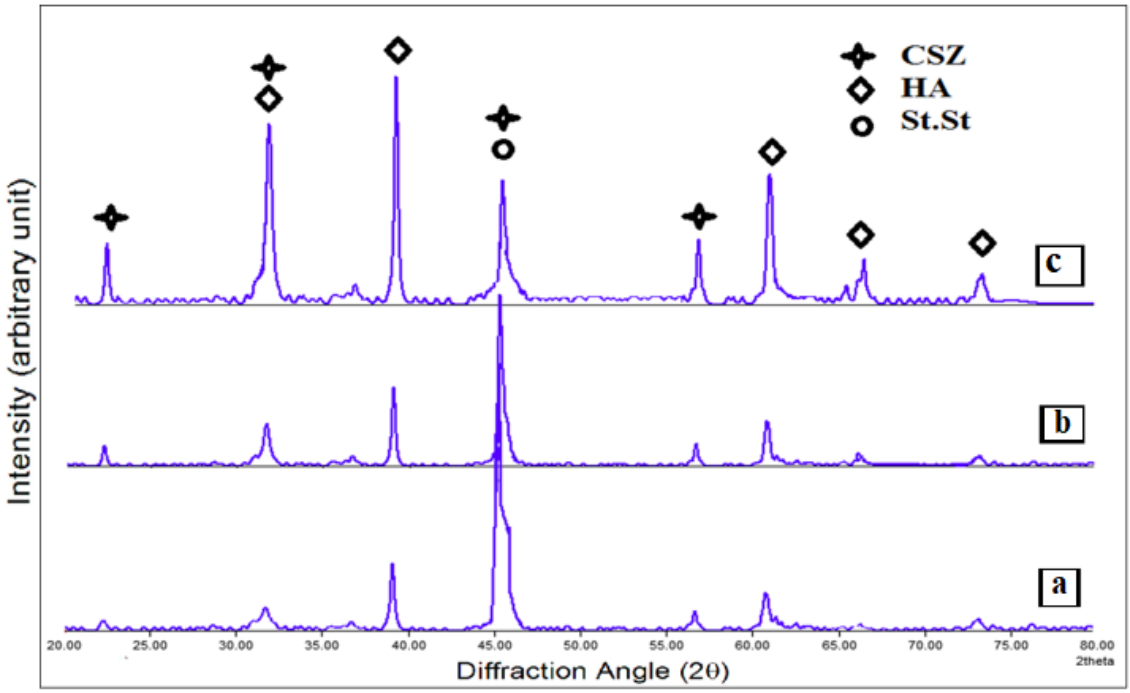

Figure 4: XRD pattern spectrum for (a) HA+1%CSZ, (b) HA+2%CSZ) and (c) HA+3%CSZ coatings.

The EDS spectra of the coatings (Figure 5) indicate the presence of several elements. Calcium (Ca) and phosphorus (P) can be observed in all coatings. Zirconium (Zr) can also be observed, which is due to the CSZ additive. As for iron (Fe), it is due to the limited coating thickness or the possibility of porosity, which may allow substrate elements to appear in the spectra. Comparison of SEM images and EDS spectra of the different coatings (Figure 5 a-d) provides insight into how increasing CSZ content affects the coating morphology and elemental distribution of 316L stainless steel. Uncoated substrate shows mainly Fe peaks associated with the base alloy composition compared to HA+1 % CSZ (Figure 5 a). Figure 5 b shows an even distribution of Ca and P, with small Zr peaks, indicating a low CSZ concentration in the matrix. SEM images show a relatively smooth morphology with minimal cracks or voids. Figure 5 c shows more pronounced zirconium peaks, indicating better integration of CSZ within the HA matrix of HA+2 % CSZ coating. SEM images reveal a denser surface, which may increase the stability and corrosion resistance of the coating. Finally HA+3 % CSZ coating (Figure 5 d) shows the highest zirconium peak intensity, indicating the presence of maximum CSZ. Elemental mapping confirms that the addition of CSZ effectively incorporates zirconium into the coating, although higher concentrations may compromise surface uniformity.

3.3. Coating thickness

Figure 6 shows that the coating thickness increases from 9.26 μm, to 11.11 μm and then to 14.34 μm with increasing CSZ concentration from1, 2 and 3 % CSZ, respectively. The increases which were clearly correlated with the HA concentration showed that the coating thickness could increase as a function of the applied voltage or deposition time. The initial period of EPD at constant voltage showed an increase in coating thickness with increasing CSZ. In addition, the cross-sections show that there is no delamination and all the coatings are located directly next to the substrate as shown in Figure 6.

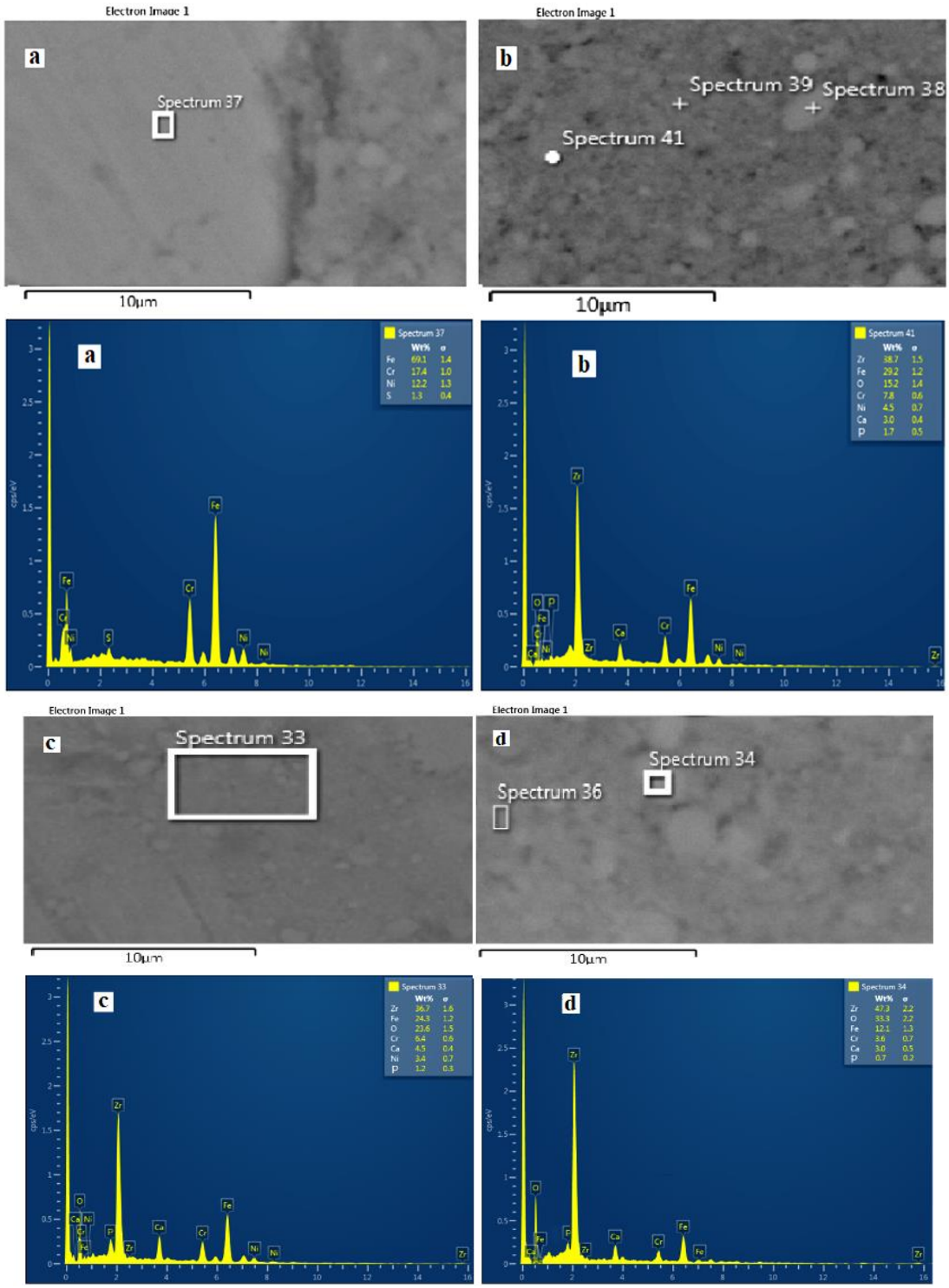

Figure 5: SEM images and EDS spectra of (a) 316 L stainless steel, and coatings of (b) HA+1 % CSZ, (c) HA+2 % CSZ) and (d) HA+3 % CSZ.

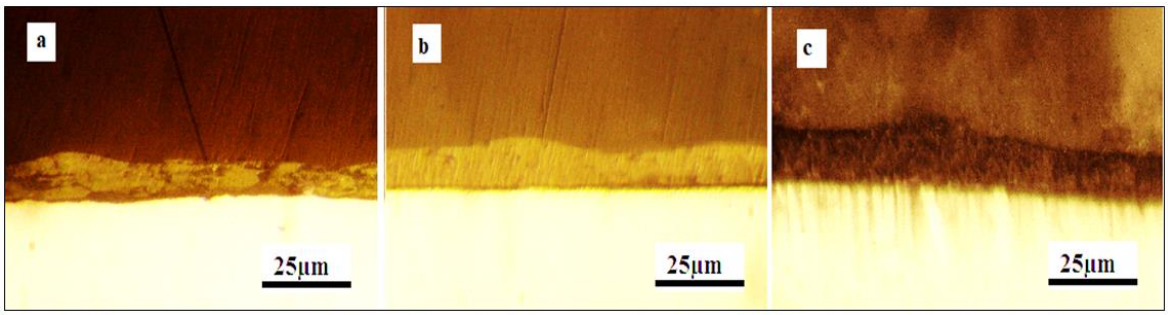

Figure 6: The EPD coatings using (a) HA+1 % CSZ, (b) HA+2 % CSZ and (c) HA+3 % CSZ.

3.4. Corrosion behavior in SBF

The electrochemical behavior of 316L stainless steel and HA-CSZ coatings is shown in Figure 7. The electrochemical behavior data are summarized in Table 3. It is clear from Figure 7 and Table 3 that the presence of HA-CSZ coating significantly improves the corrosion resistance compared to the uncoated substrate. Due to the porous structure of the coatings that can generally promote corrosion, the corrosion rate remains significantly low. This indicates that despite their structure, HA-CSZ coatings provide a degree of corrosion protection in SBF.

It is evident from Figure 7 that the anodic polarization curve shifts positively with HA-CSZ coatings, moving the potential into a more negative region. This positive shift indicates improved passivation, which reduces the material's susceptibility to corrosion. Additionally, the presence of CSZ reduces the corrosion current density, which means stronger resistance to corrosive attack. In general, CSZ forms very stable clusters within the coating, partially blocking the pores and further mitigating corrosion [34]. Previous studies on CSZ-doped hydroxyapatite coatings have shown similar benefits, although they often used thicker coatings of [35] or hydroxyapatite [36] on 316L stainless steel, a material already known for its corrosion resistance. Figure 8 highlights that even with a relatively thin layer of HA-CSZ on 316L, effective corrosion inhibition can be achieved. Thus, HA-CSZ coatings not only enhance the corrosion resistance of 316L stainless steel in SBF, but also offer a practical solution for biomedical applications where minimal thickness and improved toughness are desired.

3.5. Contact angle study

The effect of CSZ on the contact angle of different coatings can be shown in Figure 9 and Table 4. A significant decrease in the contact angle occurs with increasing concentration of CSZ bound to HA within the coating layer. Due to the known low wettability of metals, the ability of metal clusters to form Vander-Waals bonds is strongly emphasized. The sponge-like surface structure of all samples may be responsible for the low contact angles. It is clear that contact angles are indicators of wettability; lower values indicate greater potential for biocompatibility [36]. As the coating thickness increases, the crystallinity of the HA-CSZ coating with respect to the hydrophilic hydroxyl groups also increases. The EPD potential grows along with the thickness of the HA-CSZ coating. Since there are more cracks and more free space inside its porous structure, a thicker HA-CSZ coating has a lower contact angle value.

Table 3: Corrosion current density and corrosion potential of 316L stainless steel and the HA-CSZ coatings.

Sample	E_{corr} [mV]	i_{corr} [mA/Cm^2]
316L steel	-0.944488	0.00237894
HA+1 % CSZ	-1.6825	0.0141674
HA+2 % CSZ	-0.913378	0.00781608
HA+3 % CSZ	-1.45907	0.00530997

Table 4: The contact angle values for different coatings.

NO	Type of sample	Contact angle (°)
1	316L Steel	
2	HA+1 % CSZ	3.789
3	HA+2 % CSZ	2.128
4	HA+3 % CSZ	0.535

On the other hand, the presence of HA on the surface may prevent water droplets from entering the HA-CSZ coating, increasing the contact angle compared with 316L stainless steel. Therefore, the presence of 3 % HA in the HA-CSZ coating effectively enhances the surface wettability and biocompatibility.

3.6. Bonding strength

The adhesive tape test technique (single layer with surface scoop) was used for the coated samples to evaluate the qualitative bond between the coated layer and the substrate. After the adhesive test, the optical images of different coatings are shown in Figure 10. The calculations were made on a 2 mm scale to determine the percentage of coating layer loss by image J V.1.54K software. The percentage of coating removal area of three samples were determined to be 8.289, 5.435, and 3.765 %, respectively. The coating was strong when CSZ was added at different concentrations, indicating that the coating on the sandblasted surface had the best adhesion. This is a result of the removed coating area being less than 12 %. This shows that the coating layers and the substrate are well bonded.

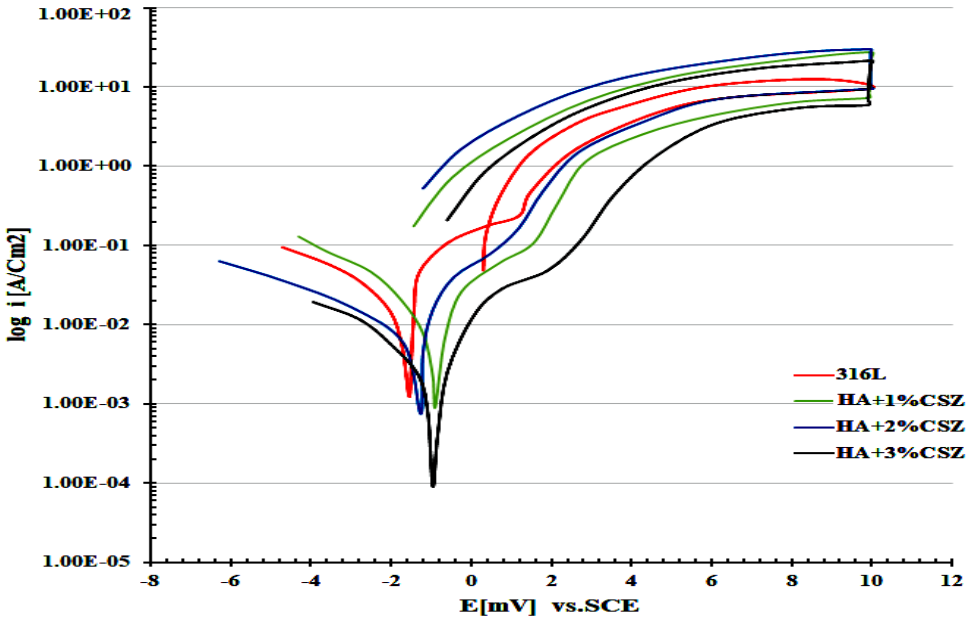

Figure 7: Cyclic polarization curves of 316 L stainless steel and HA-CSZ coatings in SBF.

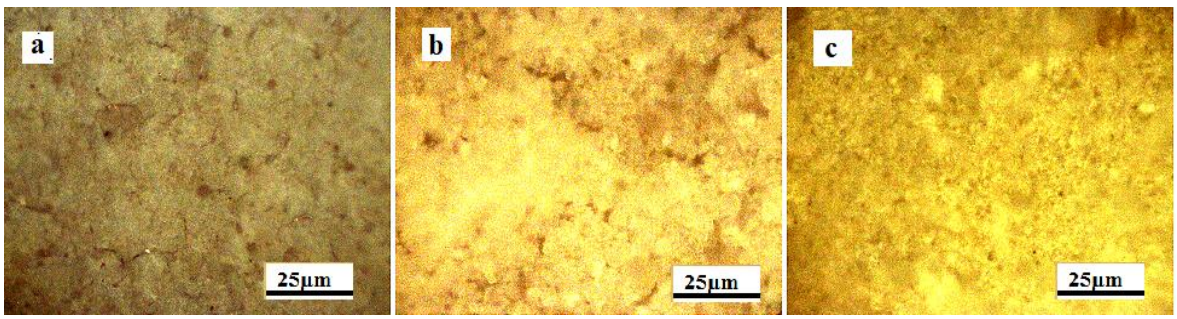

Figure 8: The corroded coatings layers in SBF of (a) HA+1 % CSZ, (b) HA+2 % CSZ and (c) HA+3 % CSZ.

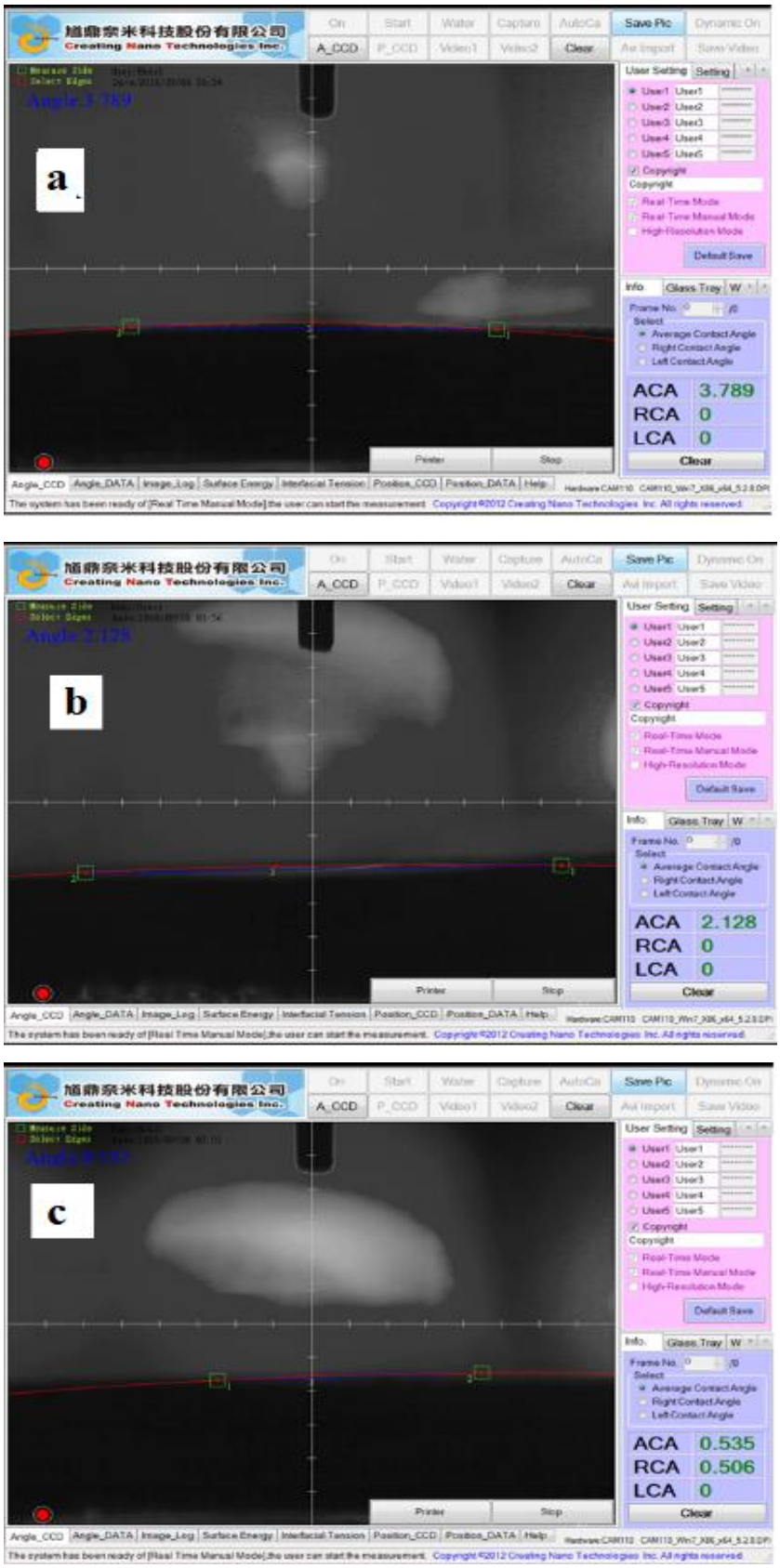

Figure 9: Sessile water contact angel measurement for different coatings (a) HA-1 % CSZ, (b) HA-2 % CSZ, and (c) HA-3 % CSZ coating.

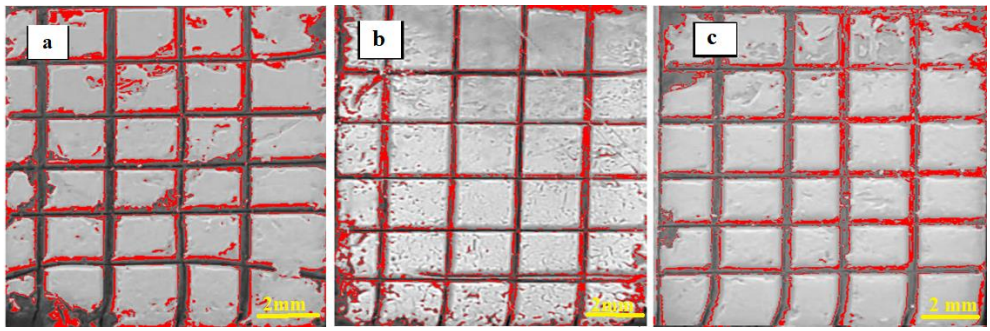

Figure10: Optical image of coating removal by tape test for (a) HA+1 % CSZ, (b) HA+2 % CSZ and (c) HA+3 % CSZ.

4. Conclusion

The EPD technique was successfully used to fabricate HA-CSZ coatings with varying CSZ concentrations, resulting in significant improvements in density, crystallinity, bond strength, and corrosion resistance. The results demonstrate the critical role of CSZ concentration in influencing the microstructure, wettability, and electrochemical behavior of the coatings as follows:

- The zeta potential increased with CSZ concentration, indicating enhanced suspension stability and homogeneity. Values of 5.28 mV for HA+1 % CSZ, 35 mV for HA+2 % CSZ, and 62 mV for HA+3 % CSZ highlight the potential for uniform and stable coatings.
- The coating thickness increased with CSZ concentration, ranging from 9.26 μm for HA+1 % CSZ to 11.11 μm and then to 14.34 μm for HA+3 % CSZ, which contributed to better surface coverage and corrosion protection.
- Significant reduction in corrosion current density (icorr) with higher CSZ levels, demonstrating improved corrosion resistance essential for durability. The i_{corr} values decreased from 0.0141674 mA/cm² for HA+1 % CSZ to 0.00530997 mA/cm² for HA+3 % CSZ.
- Contact angle measurements revealed increased hydrophilicity with higher CSZ concentration, with angles reducing from 3.789° for HA+1 % CSZ to 0.535° for HA+3 % CSZ. The enhanced wettability and biocompatibility are attributed to the sponge-like surface texture associated with higher CSZ concentrations.

5. References

1. Wang QY, Wang YB, Lin JP, Zheng YF. Development and properties of Ti–In binary alloys as dental biomaterials. Mater Sci Eng C. 2013; 33(3): 1601-1606. https://doi.org/10.1016/j.msec.2012. 12. 070.
2. Ur Rehman MA, Bastan FE, Nawaz Q, Goldmann WH, Maqbool M, Virtanen S, et al. Electrophoretic deposition of lawsone loaded bioactive glass (BG)/chitosan composite on polyetheretherketone (PEEK)/BG layers as antibacterial and bioactive coating. J Biomed Mater Res A. 2018; 106(12): 3111-3122. https://doi.org/10.1002/jbm.a.36506.
3. Abass MH, Abdulkareem MH, Hussein HA. Effect of annealing treatment on (Mg17Al12) phase characterization and corrosion behavior in different solutions for AZ91 alloy. Adv Sci Technol Res J. 2023;17(2):330–341. https://doi.org/10.12913/22998624/ 161831.
4. Abbass MK, Raheef KM, Aziz IA, Hanoon MM, Mustafa AM, Al-Azzawi WK, et al. Evaluation of 2-dimethylaminopropionamidoantipyrine as a corrosion inhibitor for mild steel in HCl solution: a combined experimental and theoretical study. Prog Color Colorants Coat. 2024;17(1):1-10. https://doi.org/10. 30509/pccc.2023.167134.1216.
5. Mohazzab BF, Jaleh B, Kakuee O, Fattah-Alhosseini A. Formation of titanium carbide on the titanium surface using laser ablation in n-heptane and investigating its corrosion resistance. Appl Surf Sci. 2019;478(1):623-635. https://doi.org/10.1016/j.apsusc. 2019.01.259.
6. Abd Muslim HW, Mundher Mustafa A, Farhan Sayyid F. Corrosion inhibition performance of whey protein-derived inhibitors for low carbon and dead mild steels in 1M hydrochloric acid. Salud, Ciencia y Tecnología - Serie de Conferencias. 2024; 3:849. https://doi. org/10.56294/sctconf2024849.
7. Ur Rehman MA, Bastan FE, Nawaz A, Nawaz Q, Wadood A. Electrophoretic deposition of PEEK/ bioactive glass composite coatings on stainless steel for orthopedic applications: an optimization for in

vitro bioactivity and adhesion strength. Inter J Adv Manufact Technol. 2020;108:1849-1862. https://doi.org/10.1007/s00170-020-05456-x.
8. Hussein MB, Mustafa AM, Abdulkareem MH. A comparative study on dip coating and corrosion behavior of Ti-13Zr-13Nb and commercially pure titanium alloys coated with YSZ by Taguchi design. Salud Cienc Tecnol-Ser Conf. 2024; 3:847. https://doi.org/10.56294/sctconf2024847.
9. Hussein MB, Mustafa AM, Abdulkareem MH, Alamiery A. Comparative corrosion performance of YSZ-coated Ti-13Zr-13Nb alloy and commercially pure titanium in orthopedic implants. S Afr J Chem Eng. 2024;48(1):40-54. https://doi.org/10.1016/j.sajce.2024.01.005.
10. Mahlooji E, Atapour M, Labbaf S. Electrophoretic deposition of bioactive glass–chitosan nanocomposite coatings on Ti-6Al-4V for orthopedic applications. Carbohydr Polym. 2019; 226:115299. https://doi.org/10.1016/j.carbpol.2019.115299.
11. Akhtar MA, Mariotti CE, Conti B, Boccaccini AR. Electrophoretic deposition of ferulic acid loaded bioactive glass/chitosan as antibacterial and bioactive composite coatings. Surf Coat Technol. 2021; 405:126657. https://doi.org/10.1016/j.surfcoat. 2020.126657.
12. Radhi NS, Salman AJ, Al-Khafaji Z. Investigation of in vitro behavior of composite coating hydroxyapatite-nano silver on 316L stainless steel substrate by electrophoretic technic for biomedical tools. Open Eng. 2024; 14(1):20240017. https://doi.org/10.1515/eng-2024-0017
13. Al-Rashidy ZM, Farag MM, Ghany NA, Ibrahim AM, Abdel-Fattah WI. Orthopaedic bioactive glass/chitosan composites coated 316L stainless steel by green electrophoretic co-deposition. Surf Coat Technol. 2018; 334:479-490. https://doi.org/10.1016/j.surfcoat.2017.11.052.
14. Shi H, Pan K, Dai M, Wei W, Liu X, Li X. A gallic acid-doped polypyrrole coating with anticorrosion and antibacterial properties on magnesium alloy. ACS Appl Bio Mater. 2022;5(9):4244-4255. https://doi.org/10.1021/acsabm.2c00453
15. Hussein MB, Abdulkareem MH, Mustafa AM. A study evaluating the improvement of the corrosion properties of a Yttria-stabilized zirconia coated on Ti-alloy by using a Taguchi design. AIP Conf Proc. 2024; 3229(1). https://doi.org/10.1063/5.0236016.
16. Sarkar S, Bhattacharjee C, Sarkar S. Smart polymeric coatings to enhance the antibacterial, anti-fogging and self-healing nature of a coated surface. Smart Polym Compos. 2018; 21:64.
17. Popoola AP, Aigbodion VS, Fayomi OS. Surface characterization, mechanical properties and corrosion behaviour of ternary based Zn–ZnO–SiO_2 composite coating of mild steel. J Alloy Compd. 2016; 654:561-566. https://doi.org/10.1016/j.jallcom.2015.09.090.
18. Bhattarai SR, Bhattarai N, Yi HK, Hwang PH, Cha DI, Kim HY. Novel biodegradable electrospun membrane: scaffold for tissue engineering. Biomaterials. 2004;25(13):2595-2602. https://doi.org/10.1016/j.biomaterials.2003.09.049.
19. Ma Y, Talha M, Guo W, Liu W, Wang Q, Zhao Q, et al. Improved corrosion protective performance of chitosan coatings reinforced with nano-ZnO on degradable magnesium alloy in simulated body fluid. Appl Phys A. 2021;127:1-2. https://doi.org/10.1007/s00339-021-05120-5.
20. Nikolova MP, Apostolova MD. Advances in multifunctional bioactive coatings for metallic bone implants. Materials. 2022;16(1):183. https://doi.org/10.3390/ma16010183
21. Sergi R, Bellucci D, Cannillo V. A review of bioactive glass/natural polymer composites: state of the art. Materials. 2020;13(23):5560. https://doi.org/10.3390/ma13235560.
22. Saranya N, Moorthi A, Saravanan S, Devi MP, Selvamurugan N. Chitosan and its derivatives for gene delivery.International J Biological Macromol. 2011;48(2):234-238. https://doi.org/10.1016/j.ijbiomac.2010.11.013.
23. Chouirfa H, Bouloussa H, Migonney VU, Falentin-Daudré C. Review of titanium surface modification techniques and coatings for antibacterial applications. Acta Biomater. 2019; 83:37-54. https://doi.org/10.1016/j.actbio.2018.10.036.
24. Abdulhasan AA, Sheng EL, Mustafa AM, Isa MR. Recent advancements in biocompatible coatings for metallic and non-metallic biomaterials: a review. Corros Sci Technol. 2024; 23(5):449-69. https://doi.org/10.14773/CST.2024.23.5.449.
25. Li Q, Zhang Y, Gong H, Sun H, Li T, Guo X, et al. Effects of graphene on the thermal conductivity of pressureless-sintered SiC ceramics. Ceram Int. 2015; 41(10):13547-52. https://doi.org/10.1016/j.ceramint.2015.07.149.
26. Mahlooji E, Atapour M, Labbaf S. Electrophoretic deposition of bioactive glass–chitosan nanocomposite coatings on Ti-6Al-4V for orthopedic applications. Carbohydr Polym. 2019; 226:115299. https://doi.org/10.1016/j.carbpol.2019.115299.
27. Tian M, Lin Z, Tang W, Wu W, Wang L, Zhang J. Electrophoretic deposition of tetracycline loaded bioactive glasses/chitosan as antibacterial and bioactive composite coatings on magnesium alloys. Prog Org Coat. 2023; 184:107841. https://doi.org/10.1016/j.porgcoat.2023.107841.
28. Drevet R, Velard F, Potiron S, Laurent-Maquin D, Benhayoune H. In vitro dissolution and corrosion study of calcium phosphate coatings elaborated by pulsed electrodeposition current on Ti6Al4V substrate. J Mater Sci Mater Med. 2011; 22:753-761. https://doi.org/10.1021/am5033908.
29. Predoi D, Iconaru SL, Predoi MV, Stan GE, Buton N. Synthesis, characterization, and antimicrobial activity of magnesium-doped hydroxyapatite suspensions. Nanomaterials. 2019; 9(9):1295. https://doi.org/10.3390/ nano9091295.

30. Allo BA, Costa DO, Dixon SJ, Mequanint K, Rizkalla AS. Bioactive and biodegradable nano-composites and hybrid biomaterials for bone regeneration. J Funct Biomater. 2012; 3(2):432-63. https://doi.org/10.3390/jfb3020432.
31. Gaharwar AK, Dammu SA, Canter JM, Wu CJ, Schmidt G. Highly extensible, tough, and elastomeric nanocomposite hydrogels from poly(ethylene glycol) and hydroxyapatite nanoparticles. Biomacromolecules. 2011;12(5):1641-1650. https://doi.org/10.1021/bm200027z.
32. Djošić M, Janković A, Mišković-Stanković V. Electrophoretic deposition of biocompatible and bioactive hydroxyapatite-based coatings on titanium. Materials. 2021; 14(18):5391. https://doi.org/10.3390/ma14185391.
33. Jasim AN, Mohammed A, Mustafa AM, Sayyid FF, Aljibori HS, Al-Azzawi WK, et al. Corrosion inhibition of mild steel in HCl solution by 2-acetylpyrazine: weight loss and DFT studies on immersion time and temperature effects. Prog Color Colorants Coat. 2024;17(4):333-350. https://doi.org/10.30509/pccc.2024.167231.1261
34. Hamood AF, Habeeb HM, Abdulhussein BA, Mustafa AM, Sayyid FF, Hanoon MM, et al. Weight loss, electrochemical measurements and DFT studies on corrosion inhibition by 7-mercapto-4-methyl-coumarin. Results Eng. 2024; 23:102677. https://doi.org/10.1016/j.rineng.2024.102677.
35. Huan Z, Fratila-Apachitei LE, Apachitei I, Duszczyk J. Porous NiTi surfaces for biomedical applications. Appl Surf Sci. 2012;258(13):5244-5249. https://doi.org/10.1016/j.apsusc.2012.02.002
36. Taha Mohamed M, Nawi SA, Mustafa AM, Sayyid FF, Hanoon MM, Al-Amiery AA, et al. Revolutionizing corrosion defense: unlocking the power of expired BCAA. Prog Color Colorants Coat. 2024; 17(2): 97-111. https://doi.org/10.30509/pccc.2023.167156.1228.

How to cite this article:
Abdulkareem MH, Dhahir Subhi A, Mustafa AM, Ali Hussein H, Adnan Annon I, Thamer Mohammed A. Corrosion Behavior and Characteristics of HA+CSZ Nano Bio Composite Coating Prepared by EPD. Prog Color Colorants Coat. 2025;18(4):397-408. https://doi.org/10.30509/pccc.2025.167464.1361.